Transactions of Tianjin University
https://doi.org/10.1007/s12209-024-00391-4

REVIEW

Coupling of BiOCl Ultrathin Nanosheets with Carbon Quantum Dots for Enhanced Photocatalytic Performance

Pin Song[1] · Xiaoyu Fang[1] · Wei Jiang[2] · Yuyang Cao[2] · Daobin Liu[2] · Shiqiang Wei[2] · Jun Du[1] · Lang Sun[1] · Lei Zhao[1] · Song Liu[2] · Yuzhu Zhou[2] · Jun Di[1,3] · Chade Lv[4] · Bijun Tang[5] · Jiefu Yang[5] · Tingting Kong[1] · Yujie Xiong[1,2]

Received: 21 December 2023 / Revised: 16 January 2024 / Accepted: 24 February 2024

Abstract

Over the past few decades, photocatalysis technology has received extensive attention because of its potential to mitigate or solve energy and environmental pollution problems.Designing novel materials with outstanding photocatalytic activities has become a research hotspot in this field. In this study, we prepared a series of photocatalysts in which BiOCl nanosheets were modified with carbon quantum dots (CQDs) to form CQDs/BiOCl composites by using a simple solvothermal method. The photocatalytic performance of the resulting CQDs/BiOCl composite photocatalysts was assessed by rhodamine B and tetracycline degradation under visible-light irradiation. Compared with bare BiOCl, the photocatalytic activity of the CQDs/BiOCl composites was significantly enhanced, and the 5 wt% CQDs/BiOCl composite exhibited the highest photocatalytic activity with a degradation efficiency of 94.5% after 30 min of irradiation. Moreover, photocatalytic N_2 reduction performance was significantly improved after introducing CQDs. The 5 wt% CQDs/BiOCl composite displayed the highest photocatalytic N_2 reduction performance to yield NH_3 (346.25 μmol/(g h)), which is significantly higher than those of 3 wt% CQDs/BiOCl (256.04 μmol/(g h)), 7 wt% CQDs/BiOCl (254.07 μmol/(g h)), and bare BiOCl (240.19 μmol/(g h)). Our systematic characterizations revealed that the key role of CQDs in improving photocatalytic performance is due to their increased light harvesting capacity, remarkable electron transfer ability, and higher photocatalytic activity sites.

Graphical Abstract

This work reports a novel CQDs/BiOCl composite photocatalyst for efficiently removing contaminants from water.

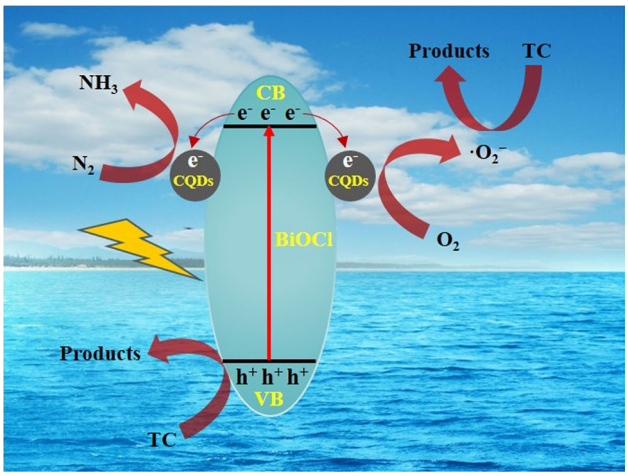

Keywords Carbon quantum dots · BiOCl · Rhodamine B · Tetracycline · Photocatalysis

Extended author information available on the last page of the article

Published online: 09 April 2024

Introduction

In recent years, ultrathin two-dimensional (2D) materials have garnered immense attention due to their excellent chemical and physical properties [1–6] and have been widely used in the fields of sensing, biological medicine, catalysis, Li-ion batteries, and supercapacitors [7–11]. For photocatalytic applications, inorganic ultrathin 2D semiconductor materials with appropriate band gaps are ideal candidates because of their superior photocatalytic performance. Traditionally, the generated charge carriers inside the material will take longer to reach the surface than surface-generated carriers [10, 12, 13]. When the same semiconductors are reduced to ultralow thickness, photogenerated carriers can be quickly transferred from the inside to the surface, thus resulting in faster charge carrier transfer. Moreover, ultrathin structure materials expose more catalytically active sites, which facilitate surface reactions [12]. Thus, constructing ultrathin 2D materials with suitable band gaps is a desirable approach for designing efficient photocatalysts.

Bismuth oxychloride (BiOCl), as a layered material with good prospects for photocatalytic energy conversion and environmental remediation, has attracted extensive attention in recent years [14–20]. BiOCl has a unique layered structure by interlacing a $[Bi_2O_2]$ slab with a double chlorine slab, which can produce a self-built internal static field and promote the separation of charge carriers [21]. So far, several strategies have been employed to prepare highly active BiOCl materials, including crystal facet exposure [22], morphology control [5, 23, 24], surface modification [19, 25, 26], and heterostructured composite construction [13, 27, 28]. Among them, the synthesis of ultrathin nanosheets is an effective approach. According to the formula $t = d^2/k^2D$ (where d, k, and D are the particle size, constant, and diffusion coefficient, respectively) [29], the ultrathin thickness of BiOCl allows a reduced d value, whereas self-built internal electric fields lead to an increased D value [30]. Thus, ultrathin BiOCl exhibits high separation efficiency of the charge carrier. Nevertheless, the photocatalytic activity of BiOCl material remains deficient. To unlock its potential for industrial applications, certain adaptations to this promising material are necessary. When selecting a material to form composites with BiOCl, the ability to develop a high-quality interface with the BiOCl matrix is a key factor to consider because interfacial defects may function as recombination centers for electron–hole pairs, resulting in adverse impacts on photocatalytic efficiency. Thus, we rationally propose carbon quantum dots (CQDs) as highly suitable candidates for reducing the formation of interfacial defects and enhancing the separation efficiency of charge carriers.

CQDs are a new type of carbon nanomaterial with a diameter of less than 10 nm and primarily contain three elements, namely, C, H, and O [31]. The surface of CQDs contains many hydroxyl, carboxyl, amino, ether, aldehyde, and other chemical functional groups. They have excellent aqueous solubility, low biotoxicity, and good biocompatibility and are widely employed in the fields of energy, biomedicine, and electrocatalysis [32]. Recently, CQDs have been introduced into photocatalytic applications due to their abundant surface functional groups and remarkable charge transfer ability. Several composite photocatalysts with high photocatalytic activity based on CQDs have been examined, such as CQDs/TiO_2 [33], CQDs/Cu_2O [34], CQDs/Ag_3PO_4 [35], and CQDs/Sb_2WO_6 [36]. However, the relationship between the structure and activity of CQDs in improving photocatalytic performance remains under debate. Because of the small size of CQDs, the interface mismatch between BiOCl nanosheets and CQDs can be significantly decreased, and CQDs/BiOCl composites with nanoscale heterojunctions can be constructed. Such a distinctive nanostructure presents several advantages. First, it amplifies the accessible area of the CQDs and BiOCl planar interface, which facilitates a fast and efficient charge transfer through the establishment of bulk-to-surface channels for electrons. Second, the remarkable dispersion of CQDs reduces the obstructive effects on light, which allows an ample influx of light into the BiOCl material and consequently maximizes its light utilization efficiency. These outstanding characteristics synergistically improve the performance and overall efficacy of the system [37]. Some systems have exhibited that nanoscale heterojunctions can significantly improve the separation of charge carriers [38–40]. Therefore, constructing a structure by modifying the BiOCl ultrathin nanosheets with CQDs for efficient photocatalysis is urgently needed.

In this work, novel CQDs/BiOCl composite photocatalysts are synthesized by a facile hydrothermal method. The structure, morphology, and photocatalytic performance are analyzed. Based on our assessment of the photocatalytic degradation of rhodamine B (RhB) and tetracycline (TC), we verify that the introduction of CQDs can significantly improve photocatalytic activity. The structure–activity relationship is systemically explored, which determines the active species that influence the photocatalytic activity, and the photocatalytic mechanism is proposed.

Results and Discussion

Figure 1a displays the X-ray diffraction (XRD) patterns for the as-prepared samples with different CQD contents. The diffraction peaks of samples at 12.0°, 25.9°, 32.6°, 33.6°, 41.0°, 46.8°, 49.9°, 54.2°, 58.8°, 68.3°, and 77.7° can be attributed to the (001), (101), (110), (102), (112), (200), (113), (121), (122), (220), and (130) planes of tetragonal

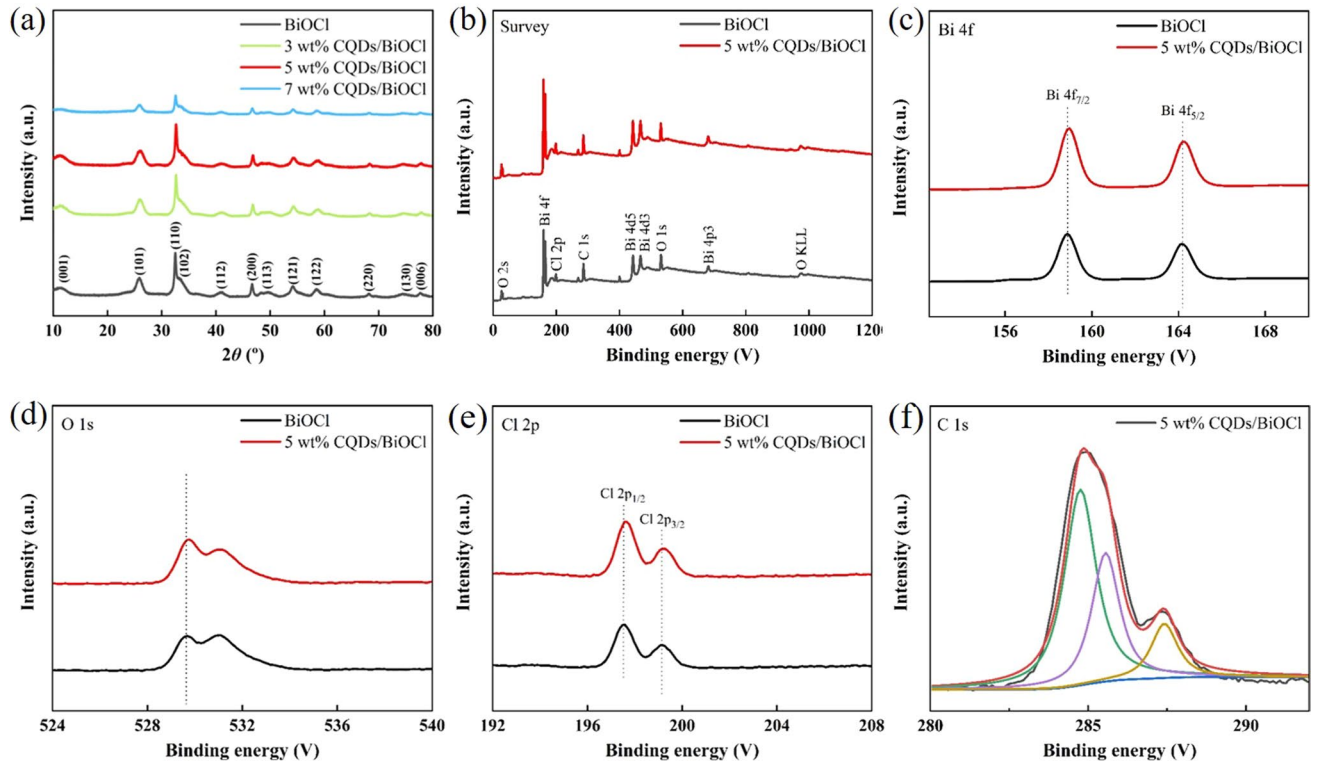

Fig. 1 **a** XRD patterns of the CQDs/BiOCl composites. XPS spectra of the CQDs/BiOCl composites: **b** survey of the sample; **c** Bi 4f; **d** O 1 s; **e** Cl 2p; **f** C 1 s

BiOCl (JCPDS card no. 73–2060), respectively. However, because of the low CQD content in the CQDs/BiOCl material, no characteristic peak of CQDs was detected in the CQDs/BiOCl material [41]. The X-ray photoelectron spectra (XPS) in Fig. 1b indicate that the as-prepared samples mainly consist of Bi, Cl, O, and C. From Fig. 1c, the characterized peaks of Bi $4f_{7/2}$ and Bi $4f_{5/2}$ were located at 158.8 eV and 164.1 eV, respectively, verifying the presence of Bi^{3+} in the as-prepared samples [42]. Due to the strong coupling between CQDs and BiOCl, the Bi 4f peaks in the 5 wt% CQDs/BiOCl sample were slightly shifted compared to those in bare BiOCl. The peak at 529.6 eV in O 1 s arose from the oxygen anions from BiOCl (Fig. 1d). Moreover, two characterized peaks were observed at 197.5 and 199.1 eV (Fig. 1e), which are ascribed to Cl $2p_{3/2}$ and Cl $2p_{1/2}$, respectively [43]. In Fig. 1f, the characterized peaks at 284.7 eV, 285.6 eV, and 287.4 eV are assigned to the C−C, C−O, and C−N, respectively [43]. The results showed that CQDs are successfully introduced into the BiOCl material. FT-IR and Raman spectra were collected to further confirm the presence of CQDs in the CQDs/BiOCl composites. Figure S1 presents the FT-IR spectra of the as-prepared samples with different CQD contents. From Fig. S1a, the peaks at 1435 cm^{-1} and 1571 cm^{-1} are ascribed to the $–COO^-$ and C=O stretching vibrations of the CQDs, respectively. After introducing CQDs, because of the interaction between CQDs and BiOCl, the $–COO^-$ and C=O stretching vibrations of CQDs shift to 1454 cm^{-1} and 1648 cm^{-1} (Fig. S1b), respectively [44]. The peak at 526 cm^{-1} is ascribed to the Bi=O stretching vibration. The Raman spectra in Fig. S2 further validate the successful introduction of CQDs into the BiOCl materials. The G band of the CQDs/BiOCl composites is stronger than the D band because the CQDs/BiOCl composite has background interference based on the strong fluorescence of the CQDs [45].

The morphology and microstructure of the as-prepared samples were further investigated by transmission electron microscopy (TEM) (Fig. S3, Fig. 2a and b). Figure S3 demonstrates that highly monodisperse CQDs are nearly spherical nanoparticles with a relatively uniform particle size distribution. The nanosheet is nearly transparent under an electron beam and has an ultrathin structure with a thickness of approximately 2 nm. Numerous nanodots can be observed, verifying the successful coupling of CQDs and BiOCl. As observed in Fig. 2c, some nanodots are uniformly attached to the BiOCl nanosheets, showing that the CQDs and BiOCl nanosheets form a good combination. However, it is difficult to observe the lattice fringes of CQDs because they have amorphous shells surrounding nanocrystalline cores [31]. To further characterize the microstructure of

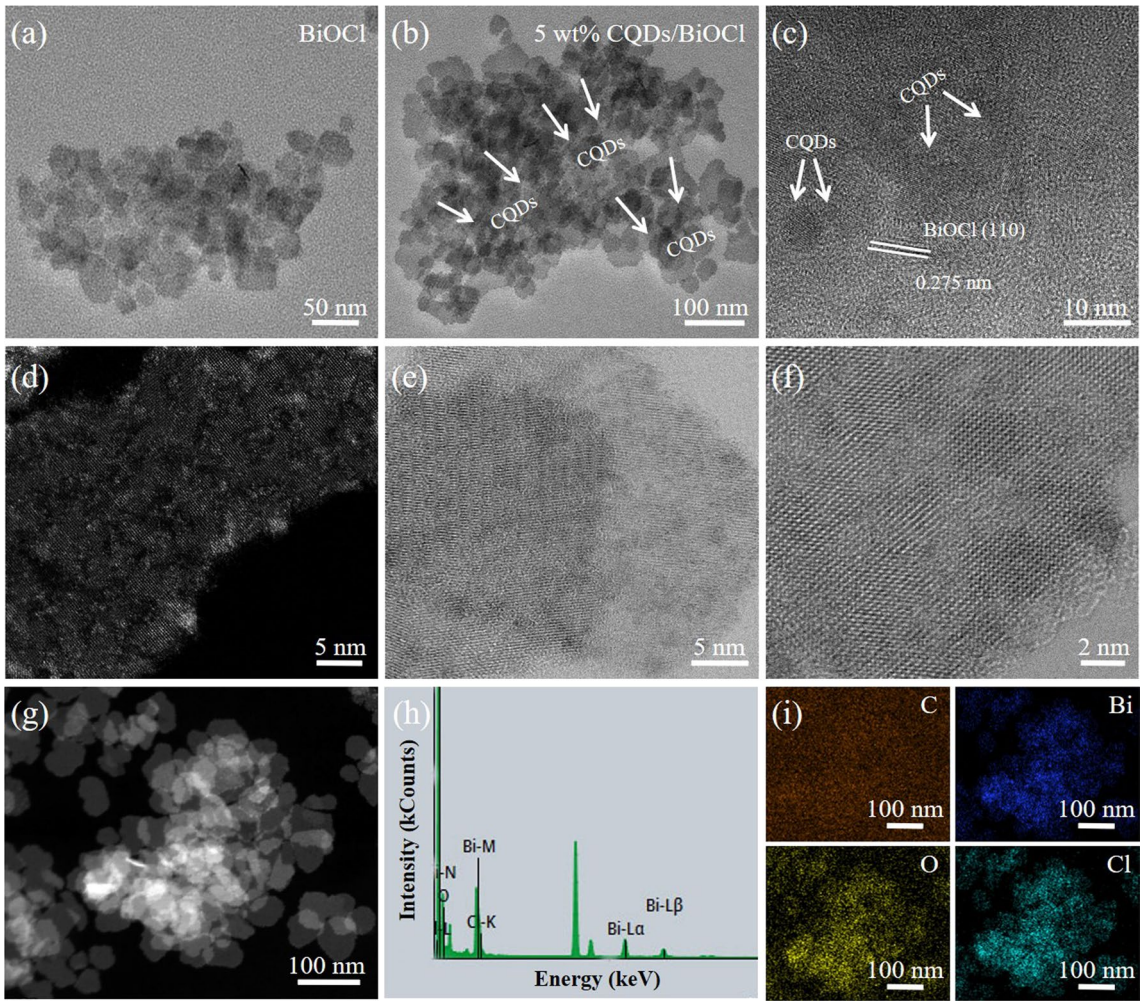

Fig. 2 **a**, **b** TEM images of BiOCl and 5 wt% CQDs/BiOCl. **c** High-magnification TEM image of 5 wt% CQDs/BiOCl. **d–f** HAADF-STEM images of 5 wt% CQDs/BiOCl. **g–i** Elemental mapping of 5 wt% CQDs/BiOCl

the 5 wt% CQDs/BiOCl composites, aberration-corrected scanning TEM with high-angle annular dark-field imaging (STEM-HAADF) was applied (Fig. 2d–f). As observed, CQDs are uniformly loaded on BiOCl. The energy-dispersive X-ray spectroscopy elemental mapping demonstrated that the Bi, Cl, O, and C are evenly distributed in the CQDs/BiOCl material (Fig. 2g–i).

The photocatalytic performance of the obtained samples was then assessed for RhB degradation under visible-light irradiation. Before the photocatalytic degradation, a blank experiment was conducted (Fig. S4). From Fig. 3a, 80.6% of RhB could be removed using bare BiOCl material after 30 min of irradiation. With the introduction of CQDs to BiOCl, the photocatalytic performance of BiOCl was significantly improved. The 5 wt% CQDs/BiOCl composite exhibited the highest photocatalytic performance with a degradation efficiency of 94.5% after 30 min of irradiation. However, a further increase in the CQD content beyond 5 wt% resulted in a decrease in photocatalytic performance. Although the modification of BiOCl with CQDs can facilitate charge transfer, excessive CQDs covering the BiOCl surface may limit light absorption [46]. The photocatalytic degradation kinetics of RhB was then examined. The reaction kinetics of RhB degradation follows the pseudo-first-order kinetics equation $-\ln(C/C_0) = kt$, where k is the relative rate constant (Fig. 3b). The rate constant of 5 wt% CQDs/BiOCl is 0.0968 min^{-1}, which is 1.77 times higher than that of bare BiOCl (Table S1). To assess the stability of the 5 wt% CQDs/BiOCl composite photocatalyst, we collected the photocatalyst after the RhB photodegradation experiment. As shown in Fig. 3c, the photocatalytic performance was well maintained after five cycles, with only a 16.3% decrease in degradation efficiency, demonstrating the high stability of the 5 wt% CQDs/BiOCl composite photocatalyst during the photocatalytic process.

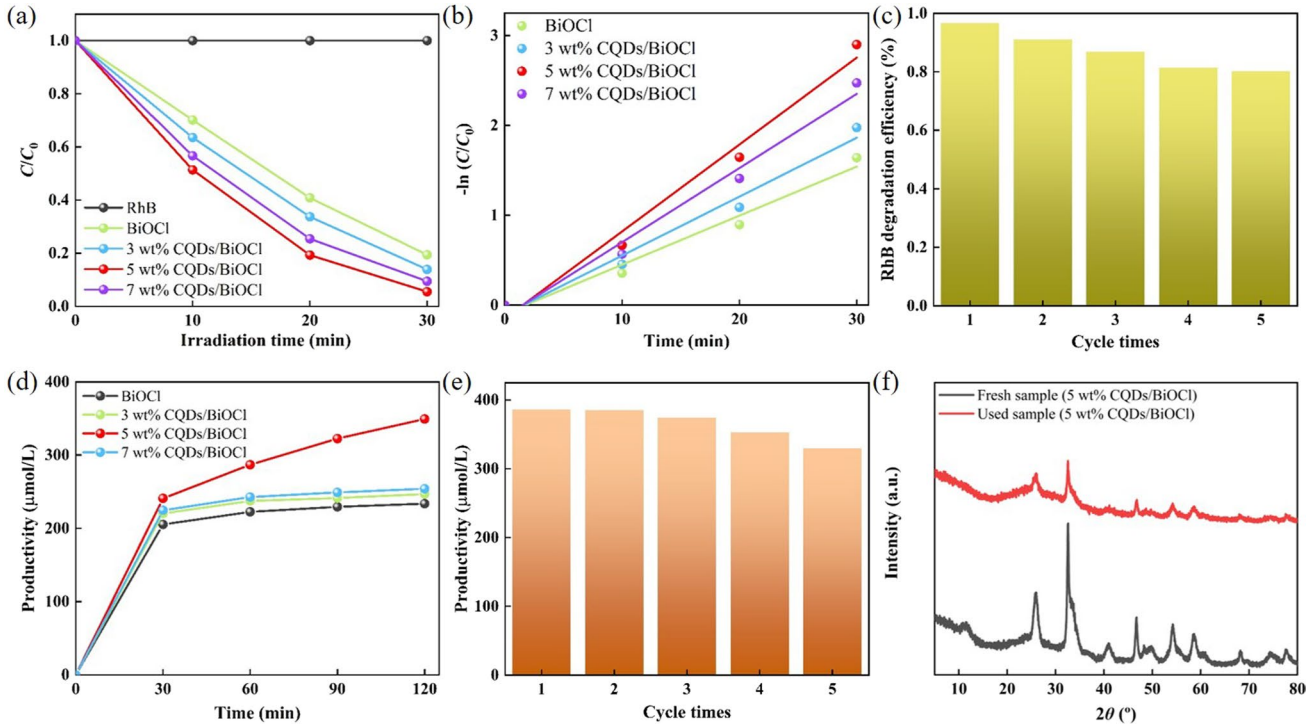

Fig. 3 **a** Photocatalytic RhB degradation. **b** Kinetic fit for the degradation of RhB. **c** Cycling runs for the photocatalytic RhB degradation over 5 wt% CQDs/BiOCl. **d** Quantitative determination of the generated ammonia. **e** Photocatalytic stability of 5 wt% CQDs/BiOCl. **f** XRD patterns of the fresh and used 5 wt% CQDs/BiOCl samples

Furthermore, TC was chosen to further assess the photocatalytic activity of the CQDs/BiOCl composite photocatalyst (Fig. S5). The bare BiOCl could remove only 57.7% of TC for 120 min. With the introduction of CQDs, the CQDs/BiOCl composite exhibited a high photocatalytic performance for TC degradation, which is an improvement of approximately 15% compared with that of bare BiOCl (Fig. S5b). The reaction kinetics of TC also follows a pseudo-first-order kinetics equation (Fig. S5c). The rate constant of 5 wt% CQDs/BiOCl is 0.0112 min^{-1}, which is significantly higher than that of bare BiOCl (0.0074 min^{-1}) (Table S2).

In parallel, we also analyzed the N_2 photoreduction performance of the as-prepared samples under light irradiation. Briefly, the catalyst (0.05 g) was dispersed in 100 mL of aqueous solution without a sacrificial agent. Under light irradiation for 120 min, the 5 wt%CQD/BiOCl composite photocatalyst exhibited the highest N_2 photoreduction performance to yield NH_3 (346.25 μmol/(g h)), which is 1.3 times (256.04 μmol/(g h)) of 3 wt% CQDs/BiOCl, 1.4 times (254.07 μmol/(g h)) of 7 wt% CQDs/BiOCl, and 1.5 times (240.19 μmol/(g h)) of BiOCl (Fig. 3d). Figure 3e indicates that the 5 wt% CQDs/BiOCl composite photocatalyst can retain 86% photocatalytic activity even after five consecutive cycles. To assess the stability of the catalyst, we collected the photocatalysts after the reaction. The crystal structure of the 5 wt% CQDs/BiOCl composite photocatalyst has no obvious change (Fig. 3f), and the CQDs are still well distributed on the surface of BiOCl (Fig. S6). To further confirm the structural stability of CQDs/BiOCl, we recorded the FT-IR spectra of the 5 wt% CQDs/BiOCl composite photocatalyst after the reactions, and the findings indicate no significant change (Fig. S7). These results validate that the CQDs/BiOCl composite photocatalyst has remarkable photocatalytic stability.

To disclose the fundamental role of CQDs in performance improvement, the optical absorption of the obtained samples was determined by UV–Vis absorption spectroscopy. As found in Fig. 4a, the bare BiOCl material only has light absorption in the UV and visible-light regions, with an absorption edge of 550 nm. With the introduction of CQDs into BiOCl, the CQDs/BiOCl composite photocatalyst showed a wide visible-light absorption region. The results indicate that the introduction of CQDs into BiOCl can improve light absorption, thus improving the photocatalytic performance [47]. The O K-edge X-ray absorption near edge structure spectra of BiOCl and 5 wt% CQDs/BiOCl are shown in Fig. S8. Compared to BiOCl, 5 wt% CQDs/BiOCl exhibits a shift toward lower energy, implying that the coordination environment and charge distribution of O have changed, which is mainly ascribed to oxygen vacancies. The specific surface area (SSA) and pore size distribution were determined from the N_2 adsorption/desorption

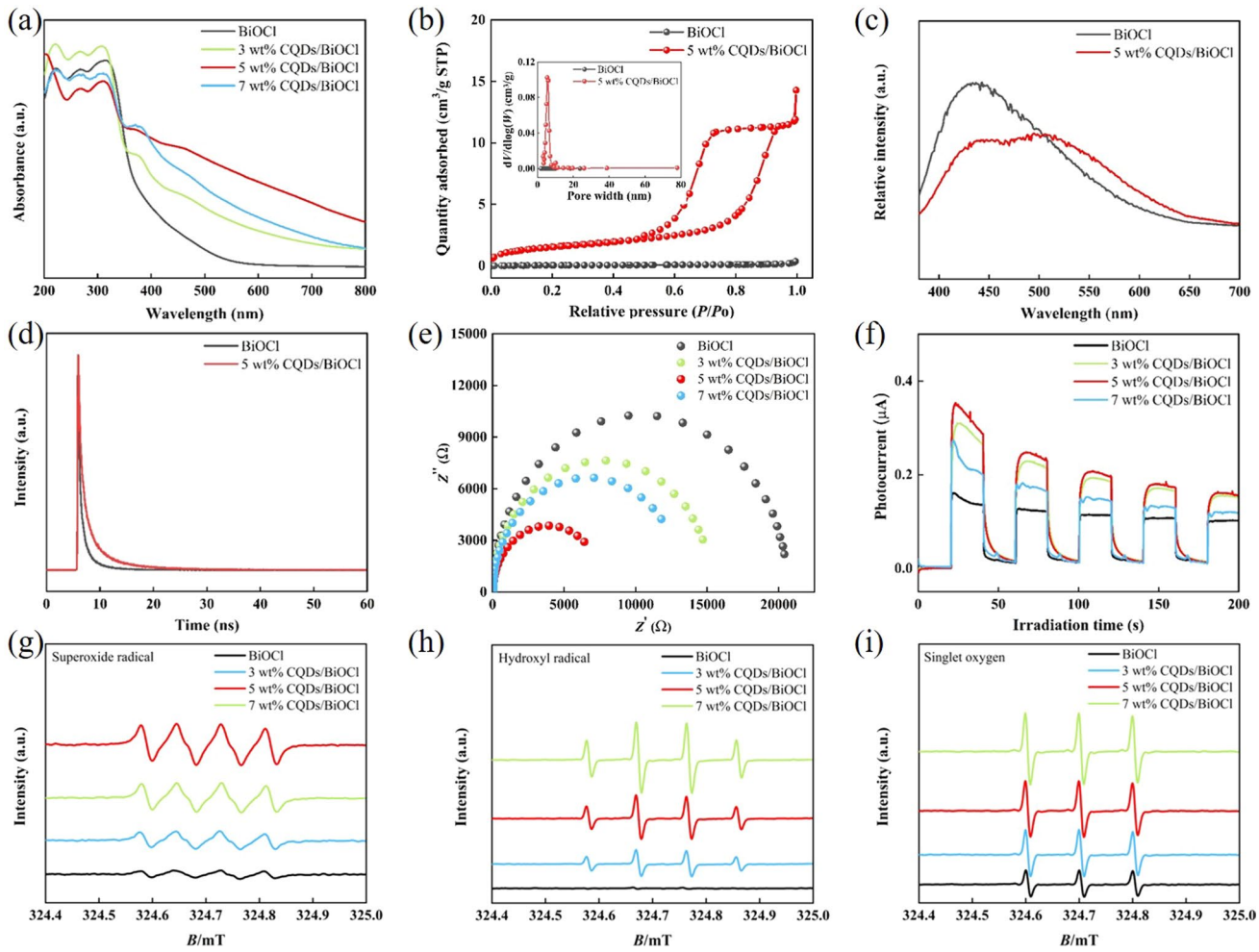

Fig. 4 **a** UV–Vis absorption spectra. **b** Nitrogen absorption/desorption isotherms. **c** Steady-state PL spectra. **d** Time-resolved transient PL decay. **e** EIS spectra. **f** Transient photocurrent response. **g**, **h** ESR spectra of the DMPO-·O_2^- adducts and DMPO-·OH recorded. **i** Singlet oxygen spectra by ESR

isotherms (Fig. 4b). As shown in Fig. 4b, the SSA of 5 wt% CQDs/BiOCl (5.73 m^2/g) was higher than that of bare BiOCl (0.20 m^2/g). Generally, a higher SSA allows the surface of materials to absorb more active species, leading to a higher photocatalytic activity [48]. Photoluminescence (PL) spectra were then measured to investigate the transfer and recombination processes of the photogenerated electron–hole pairs. From Fig. 4c, the PL intensity of 5 wt% CQDs/BiOCl was substantially decreased compared with that of bare BiOCl, corroborating that the introduction of CQDs can effectively suppress charge carrier recombination [49]. Time-resolved transient photoluminescence spectroscopy was utilized to explore the dynamic processes (Fig. 4d). The lifetime of charge carriers for 5 wt% CQDs/BiOCl was clearly longer than that of bare BiOCl, further implying a lower recombination rate of charge carriers. Figure S9 displays the PL spectrum of CQDs. Notably, when the excitation wavelength is 532 nm in the visible-light region, CQDs can produce emission at 220 nm in the UV region. The results show that the CQDs have remarkable upconversion PL performance. By integrating BiOCl with CQDs, visible light can be converted into high-energy UV light, thus exciting BiOCl and enhancing visible-light absorption.

Electron paramagnetic resonance spectroscopy was further employed to monitor the generation of oxygen vacancies in the as-prepared samples. In Fig. S10, both BiOCl and 5 wt% CQDs/BiOCl have oxygen vacancy defects, and the signal of CQDs/BiOCl is stronger than that of BiOCl, demonstrating that the introduction of CQDs increases the oxygen vacancies. It has been verified that increasing the oxygen vacancies can effectively optimize the photocatalytic performance of CQDs/BiOCl [50]. Electrochemical impedance spectroscopy (EIS) was used to examine the charge transfer processes. Generally, the small semicircle in the plot indicates low resistance [51]. Figure 4e demonstrates that CQDs/BiOCl has a lower resistance than bare BiOCl. This

suggests that the interfacial charge transfer is facilitated by the introduction of CQDs, resulting in the effective separation of charge carriers [52]. To better explain the mechanism, transient photocurrent experiments were performed. As observed in Fig. 4f, the photocurrent of the CQDs/BiOCl electrode is clearly higher than that of the bare BiOCl electrode. These results show that the introduction of CQDs can boost charge separation [53], which is consistent with the above PL and EIS results.

To gain information on the photocatalytic mechanism from the viewpoint of chemistry, we resolved the active species that were generated by the as-prepared samples during the photodegradation process by using electron spin resonance (ESR) with 5,5-dimethy-1-pyrroline N-oxide as a spin-trapping agent [54]. As shown in Fig. 4g, the superoxide radical ($\cdot O_2^-$) was observed for the as-prepared materials under visible-light irradiation. The $\cdot O_2^-$ intensity of the CQDs/BiOCl composite was significantly higher than that of bare BiOCl (Fig. 4g). As the generation of $\cdot O_2^-$ originates from O_2 reduction through one-electron transfer, the higher $\cdot O_2^-$ intensity of the CQDs/BiOCl composites confirms that CQDs allow more photogenerated electrons to reduce O_2. In fact, the delocalized conjugated structure of CQDs allows them to transfer photogenerated electrons easily [55]. From Fig. 4h, the hydroxyl radical (·OH) was also detected under visible-light irradiation, and the generated amounts of ·OH were increased with increasing CQD content. Moreover, Fig. 4i displays the singlet oxygen spectra of the as-prepared samples under UV irradiation. The generated amounts of singlet oxygen by CQDs/BiOCl were increased with increasing in CQD content, which is beneficial for the removal of pollutants. Catalytic measurements have revealed that the CQDs/BiOCl material can be utilized as an efficient photocatalytic degradation system. However, it is still unclear how the photocatalytic process works. To decode the mechanism, a series of control experiments were conducted to analyze the process (Fig. S11). Only 8.7% and 10.5% of TC degradation occurred in the absence of the catalyst and light, respectively, indicating that light and catalyst are indeed required for the reaction. When the reaction was conducted under an argon atmosphere, 56.3% of TC was degraded, which should be driven by photogenerated holes. To determine the types of reactive oxygen species responsible for photocatalytic degradation in our system, we performed characterization using different scavengers, confirming that photogenerated holes are indispensable for the photocatalytic degradation of TC. The control experiment also showed that the reaction activity is largely suppressed using Na_2S as a hole scavenger. Moreover, $\cdot O_2^-$ was confirmed to play a significant role in the photocatalytic oxidation reaction by ESR analysis (Fig. 4g) and free radical trapping experiments (Fig. S11).

Moreover, the valence band (VB) and conduction band (CB) potentials were calculated using $E_{CB} = E_{VB} - E_g$, where E_{VB} is the VB edge potential, E_{CB} is the CB edge potential, and E_g is the band gap energy. As observed in Fig. S12, the E_g value of 5 wt% CQDs/BiOCl was 2.92 eV. Figure S13 shows that the E_{VB} value of 5 wt% CQDs/BiOCl was 1.21 eV. From $E_{CB} = E_{VB} - E_g$, the E_{CB} value of 5 wt% CQDs/BiOCl was calculated to be − 1.71 eV. Here, electrons with energy above E_{CB} (− 1.71 eV) can reduce O_2 to generate $\cdot O_2^-$ because $E^0(O_2/\cdot O_2^-)$ is − 0.046 eV (vs. NHE) [56, 57]. From the above discussion and results, the mechanism of organic pollutant degradation was proposed, as illustrated in Fig. S14. CQDs with remarkable electrical conductivity were introduced into the BiOCl materials as charge mediators. Due to the bridge effect between the two substances, the separation efficiency of the change carriers was significantly enhanced, which offers more electrons to generate the $\cdot O_2^-$ active species. Moreover, CQDs can also absorb light at longer wavelengths than BiOCl [58], extending the range of light absorption. Thus, the photocatalytic activity of CQDs/BiOCl was significantly improved after the introduction of CQDs.

Conclusions

In this work, a novel CQDs/BiOCl composite photocatalyst was prepared by using a facile hydrothermal method. The CQDs were integrated on the surface of the BiOCl ultrathin nanosheets to form a tight junction. After introducing CQDs, the photocatalytic activity of the CQDs/BiOCl composites in RhB and TC degradation was significantly enhanced under visible-light irradiation. The 5 wt% CQDs/BiOCl material exhibited the highest photocatalytic performance with a degradation efficiency of 94.5% after 30 min of irradiation. Moreover, the N_2 photoreduction performance was significantly improved after introducing CQDs. The 5 wt% CQDs/BiOCl demonstrated a nitrogen photoreduction performance to yield NH_3 of 346.25 μmol/(g h), which is significantly higher than those of 3 wt% CQDs/BiOCl (256.04 μmol/(g h)), 7 wt% CQDs/BiOCl (254.07 μmol/(g h)), and bare BiOCl (240.19 μmol/(g h)). The key role of CQDs in improving photocatalytic performance was ascribed to their increased light harvesting capacity, outstanding electron transfer ability, and higher photocatalytic active sites. From the ESR and free radical trapping analysis results, holes and $\cdot O_2^-$ were the main active species. This study provides insights into the design of composite photocatalysts by integrating 2D materials and quantum dots.

Supplementary Information The online version contains supplementary material available at https://doi.org/10.1007/s12209-024-00391-4.

Acknowledgements This work was financially supported by Key Research and Development Project of Anhui Province (No. 2023h11020002), Natural Science Research Project for Universities

in Anhui Province (No. KJ2021ZD0006), Natural Science Foundation of Anhui Province (No. 2208085MB21), Fundamental Research Funds for the Central Universities of China (No. PA2022GDSK0056), Anhui Laboratory of Molecule-Based Materials (No. fzj22009), and National Natural Science Foundation of China (Nos. 21725102, 22205108).

Declarations

Conflict of interest All authors declare that there are no competing interests.

References

1. Choi SH, Yun SJ, Won YS et al (2022) Large-scale synthesis of graphene and other 2D materials towards industrialization. Nat Commun 13(1):1484
2. Li L, Xia Y, Zeng M et al (2022) Facet engineering of ultrathin two-dimensional materials. Chem Soc Rev 51(17):7327–7343
3. Zhou Y, Xu L, Liu M et al (2022) Viscous solvent-assisted planetary ball milling for the scalable production of large ultrathin two-dimensional materials. ACS Nano 16(7):10179–10187
4. Peng J, Dong W, Wang Z et al (2020) Recent advances in 2D transition metal compounds for electrocatalytic full water splitting in neutral media. Mater Today Adv 8:100081
5. Di J, Chen C, Zhu C et al (2019) Bismuth vacancy-tuned bismuth oxybromide ultrathin nanosheets toward photocatalytic CO_2 reduction. ACS Appl Mater Interfaces 11(34):30786–30792
6. Song P, Wang M, Di J et al (2020) Reusable graphitic carbon nitride nanosheet-based aerogels as sorbents for oils and organic solvents. ACS Appl Nano Mater 3(8):8176–8181
7. Sun Y, Gao S, Xie Y (2014) Atomically-thick two-dimensional crystals: electronic structure regulation and energy device construction. Chem Soc Rev 43(2):530–546
8. Zhou Y, Song P, Pan M et al (2023) Super hydrophilic-electrons acceptor regulated rutile TiO_2 nanorods for promoting photocatalytic H_2 evolution. Appl Surf Sci 623:157098
9. Zhang J, Song X, Wang L et al (2021) Ultrathin two-dimensional hybrid perovskites toward flexible electronics and optoelectronics. Natl Sci Rev 9(5):nwab129
10. Shao T, Wang X, Dong H et al (2022) A stacked plasmonic metamaterial with strong localized electric field enables highly efficient broadband light-driven CO_2 hydrogenation. Adv Mater 34(28):e2202367
11. Song P, Di J, Chen H et al (2020) A three-dimensional porous MoS_2–PVP aerogel as a highly efficient and recyclable sorbent for oils and organic solvents. Mater Adv 1(4):760–766
12. Sun Y, Sun Z, Gao S et al (2012) Fabrication of flexible and freestanding zinc chalcogenide single layers. Nat Commun 3:1057
13. Zhang JJ, Di J, Zhao YP et al (2023) Synergistic defect and doping engineering building strong bonded S-scheme heterojunction for photocatalysis. Chemosphere 344:140347
14. Liang H, Song P, Jiang W et al (2023) Indium-based atomic layer for photoreduction reactions: design, synthesis and performance optimization. Sep Purif Technol 324:124514
15. Xiong J, Song P, Di J et al (2020) Atomic-level active sites steering in ultrathin photocatalysts to trigger high efficiency nitrogen fixation. Chem Eng J 402:126208
16. Di J, Chen C, Zhu C et al (2021) Cobalt nitride as a novel cocatalyst to boost photocatalytic CO_2 reduction. Nano Energy 79:105429
17. Yao L, Yang H, Chen Z et al (2020) Bismuth oxychloride-based materials for the removal of organic pollutants in wastewater. Chemosphere 273:128576
18. Dong Y, Pang S, Zhang F et al (2023) A novel lateral epitaxial Bi_2O_3@BiOCl heterostructure for photocatalytic antibiotic degradation in an internal circulation fluidized bed reactor. Chem Eng J 478:147540
19. Li Q, Ren J, Hao YJ et al (2022) Insight into reactive species-dependent photocatalytic toluene mineralization and deactivation pathways via modifying hydroxyl groups and oxygen vacancies on BiOCl. Appl Catal B Environ 317:121761
20. Song P, Du J, Ma X et al (2023) Design of $Bi_4O_5Br_2$/g-C_3N_4 heterojunction for efficient photocatalytic removal of persistent organic pollutants from water. EcoEnergy 1(1):197–206
21. Zhao K, Zhang L, Wang J et al (2013) Surface structure-dependent molecular oxygen activation of BiOCl single-crystalline nanosheets. J Am Chem Soc 135(42):15750–15753
22. Li ZQ, Chen XH, Li T et al (2023) Crystal facet engineering of polar single crystal BiOCl with improved piezo-photocatalytic activity. Appl Surf Sci 615:156283
23. Cao D, Xu W, Chen S et al (2023) Visualizing catalytic dynamics processes via synchrotron radiation multitechniques. Adv Mater 35(30):e2205346
24. Liu C, Ren Y, Wang Z et al (2022) Flowerlike BiOCl nanospheres fabricated by an in situ self-assembly strategy for efficiently enhancing photocatalysis. J Colloid Interface Sci 607(Pt 1):423–430
25. Cong W, Song P, Zhang Y et al (2022) Supramolecular confinement pyrolysis to carbon-supported Mo nanostructures spanning four scales for hydroquinone determination. J Hazard Mater 437:129327
26. Ma ZP, Zhang L, Ma X et al (2022) A dual strategy for synthesizing crystal plane/defect co-modified BiOCl microsphere and photodegradation mechanism insights. J Colloid Interface Sci 617:73–83
27. Senasu T, Lorwanishpaisarn N, Hemavibool K et al (2023) Construction of g-C_3N_4/BiOCl/CdS heterostructure photocatalyst for complete removal of oxytetracycline antibiotic in wastewater. Sep Purif Technol 306:122735
28. Lin B, Chaturvedi A, Di J et al (2020) Ferroelectric-field accelerated charge transfer in 2D $CuInP_2S_6$ heterostructure for enhanced photocatalytic H_2 evolution. Nano Energy 76:104972
29. Sun Y, Cheng H, Gao S et al (2012) Freestanding tin disulfide single-layers realizing efficient visible-light water splitting. Angew Chem Int Ed Engl 51(35):8727–8731
30. Jiang J, Zhao K, Xiao X et al (2012) Synthesis and facet-dependent photoreactivity of BiOCl single-crystalline nanosheets. J Am Chem Soc 134(10):4473–4476

31. Lim SY, Shen W, Gao Z (2015) Carbon quantum dots and their applications. Chem Soc Rev 44(1):362–381
32. Guo Y, Zhang R, Zhang S et al (2022) Ultrahigh oxygen-doped carbon quantum dots for highly efficient H_2O_2 production via two-electron electrochemical oxygen reduction. Energy Environ Sci 15(10):4167–4174
33. Ding C, Guo J, Chen P et al (2022) All-solid-state Z-scheme In_2S_3/CQDs/TiO_2 heterojunction for highly efficient degradation of ofloxacin. Appl Surf Sci 596:153629
34. Li H, Liu R, Liu Y et al (2012) Carbon quantum dots/Cu_2O composites with protruding nanostructures and their highly efficient (near) infrared photocatalytic behavior. J Mater Chem 22(34):17470–17475
35. Shao N, Hou Z, Zhu H et al (2018) Novel 3D core-shell structured CQDs/Ag_3PO_4@Benzoxazine tetrapods for enhancement of visible-light photocatalytic activity and anti-photocorrosion. Appl Catal B Environ 232:574–586
36. Li W, Wang Z, Li Y et al (2022) Visible-NIR light-responsive 0D/2D CQDs/Sb_2WO_6 nanosheets with enhanced photocatalytic degradation performance of RhB: unveiling the dual roles of CQDs and mechanism study. J Hazard Mater 424(Pt C):127595
37. Hou Y, Laursen AB, Zhang J et al (2013) Layered nanojunctions for hydrogen-evolution catalysis. Angew Chem Int Ed Engl 52(13):3621–3625
38. Yu C, Li G, Kumar S et al (2014) Phase transformation synthesis of novel Ag_2O/Ag_2CO_3 heterostructures with high visible light efficiency in photocatalytic degradation of pollutants. Adv Mater 26(6):892–898
39. Yu C, Yang K, Xie Y et al (2013) Novel hollow Pt-ZnO nanocomposite microspheres with hierarchical structure and enhanced photocatalytic activity and stability. Nanoscale 5(5):2142–2151
40. Xu M, Yu R, Guo Y et al (2019) New strategy towards the assembly of hierarchical heterostructures of SnO_2/ZnO for NO_2 detection at a ppb level. Inorg Chem Front 6(10):2801–2809
41. Di J, Xia J, Ge Y et al (2015) Novel visible-light-driven CQDs/Bi_2WO_6 hybrid materials with enhanced photocatalytic activity toward organic pollutants degradation and mechanism insight. Appl Catal B Environ 168–169:51–61
42. Di J, Xia J, Yin S et al (2014) Preparation of sphere-like g-C_3N_4/BiOI photocatalysts via a reactable ionic liquid for visible-light-driven photocatalytic degradation of pollutants. J Mater Chem A 2(15):5340–5351
43. Zhu S, Meng Q, Wang L et al (2013) Highly photoluminescent carbon dots for multicolor patterning, sensors, and bioimaging. Angew Chem Int Ed Engl 52(14):3953–3957
44. Duo F, Wang Y, Fan C et al (2016) Enhanced visible light photocatalytic activity and stability of CQDs/BiOBr composites: the upconversion effect of CQDs. J Alloys Compd 685:34–41
45. Xia J, Di J, Li H et al (2016) Ionic liquid-induced strategy for carbon quantum dots/BiOX (X = Br, Cl) hybrid nanosheets with superior visible light-driven photocatalysis. Appl Catal B Environ 181:260–269
46. Di J, Xia J, Ji M et al (2015) The synergistic role of carbon quantum dots for the improved photocatalytic performance of Bi_2MoO_6. Nanoscale 7(26):11433–11443
47. Gao X, Wu HB, Zheng L et al (2014) Formation of mesoporous heterostructured $BiVO_4$/Bi_2S_3 hollow discoids with enhanced photoactivity. Angew Chem Int Ed Engl 53(23):5917–5921
48. Di J, Xia J, Yin S et al (2014) One-pot solvothermal synthesis of Cu-modified BiOCl via a Cu-containing ionic liquid and its visible-light photocatalytic properties. RSC Adv 4(27):14281–14290
49. Wang S, Li D, Sun C et al (2014) Synthesis and characterization of g-C_3N_4/Ag_3VO_4 composites with significantly enhanced visible-light photocatalytic activity for triphenylmethane dye degradation. Appl Catal B Environ 144:885–892
50. Gu X, Yan Q, Wei Y et al (2019) Visible-light-responsive photocatalyst with a microsphere structure: preparation and photocatalytic performance of CQDs@BiOCl. J Mater Sci Mater Electron 30(17):16321–16336
51. Leelavathi A, Madras G, Ravishankar N (2014) New insights into electronic and geometric effects in the enhanced photoelectrooxidation of ethanol using ZnO nanorod/ultrathin Au nanowire hybrids. J Am Chem Soc 136(41):14445–14455
52. Zhu Y, Ji X, Pan C et al (2013) A carbon quantum dot decorated RuO_2 network: outstanding supercapacitances under ultrafast charge and discharge. Energy Environ Sci 6(12):3665–3675
53. Di J, Xia J, Yin S et al (2013) A g-C_3N_4/BiOBr visible-light-driven composite: synthesis via a reactable ionic liquid and improved photocatalytic activity. RSC Adv 3(42):19624–19631
54. Lv Y, Zhu Y, Zhu Y (2013) Enhanced photocatalytic performance for the $BiPO_{4-x}$ nanorod induced by surface oxygen vacancy. J Phys Chem C 117(36):18520–18528
55. Hu Q, Ji M, Di J et al (2018) Ionic liquid-induced double regulation of carbon quantum dots modified bismuth oxychloride/bismuth oxybromide nanosheets with enhanced visible-light photocatalytic activity. J Colloid Interface Sci 519:263–272
56. Ye L, Chen J, Tian L et al (2013) BiOI thin film via chemical vapor transport: photocatalytic activity, durability, selectivity and mechanism. Appl Catal B Environ 130–131:1–7
57. Chen C, Ma W, Zhao J (2010) Semiconductor-mediated photodegradation of pollutants under visible-light irradiation. Chem Soc Rev 39(11):4206–4219
58. Yu C, Wei L, Zhou W et al (2014) Enhancement of the visible light activity and stability of Ag_2CO_3 by formation of AgI/Ag_2CO_3 heterojunction. Appl Surf Sci 319:312–318

Pin Song received his Ph.D. under the supervision of Prof. Shu-Hong Yu from Hefei University of Technology (HFUT) in 2018. He carried out postdoctoral research (2018–2021) at Nanyang Technological University with Professor Zheng Liu. Then, he joined Professor Yujie Xiong's team as a professor at Anhui Normal University. His research interests mainly focus on the synthesis of novel two dimensional materials and the application for photocatalytic energy conversion, and the research of new photocatalysis technology based on 3D printing

Jun Di received his BS degree in (2012) and Ph.D. degree (2018) from Jiangsu University. He then carried out postdoctoral research (2018–2022) at Nanyang Technological University with Professor Zheng Liu. He is a professor at Nanjing University of Science and Technology. He is the first or corresponding author of more than 70 peer-reviewed scientific papers published on Nat. Commun., Coord. Chem. Rev., Adv. Mater., Angew. Chem. Int. Ed., Mater. Today, etc., with over 12000 citations and H-index of 61. His research interests focus on design and synthesis of 2D materials for photocatalytic energy conversion.

Yujie Xiong received his B.S. in chemical physics in 2000 and Ph.D. in inorganic chemistry in 2004, both from the University of Science and Technology of China (USTC). From 2004 to 2009, he worked as a Postdoctoral Fellow at the University of Washington in Seattle and as a Research Associate at the University of Illinois at Urbana-Champaign, respectively. He was the Principal Scientist of the National Nanotechnology Infrastructure Network (NSF-NNIN) site at Washington University in St. Louis in 2009–2011. He joined the USTC faculty in 2011, and currently, is the Chair Professor of Chemistry. His research centers on solar-driven artificial carbon cycle.

Authors and Affiliations

Pin Song[1] · Xiaoyu Fang[1] · Wei Jiang[2] · Yuyang Cao[2] · Daobin Liu[2] · Shiqiang Wei[2] · Jun Du[1] · Lang Sun[1] · Lei Zhao[1] · Song Liu[2] · Yuzhu Zhou[2] · Jun Di[1,3] · Chade Lv[4] · Bijun Tang[5] · Jiefu Yang[5] · Tingting Kong[1] · Yujie Xiong[1,2]

✉ Pin Song
songpin@ahnu.edu.cn

✉ Jun Di
dijun@njust.edu.cn

✉ Yujie Xiong
yjxiong@ustc.edu.cn

[1] Key Laboratory of Functional Molecular Solids, Ministry of Education, Anhui Engineering Research Center of Carbon Neutrality, College of Chemistry and Materials Science, Anhui Normal University, Wuhu 241000, China

[2] National Synchrotron Radiation Laboratory, CAS Center for Excellence in Nanoscience, School of Chemistry and Materials Science, University of Science and Technology of China, Hefei 230029, China

[3] School of Chemistry and Chemical Engineering, National Special Superfine Powder Engineering Research Center, Nanjing University of Science and Technology, Nanjing 210094, China

[4] MIIT Key Laboratory of Critical Materials Technology for New Energy Conversion and Storage, School of Chemistry and Chemical Engineering, Harbin Institute of Technology, Harbin 150001, China

[5] School of Materials Science & Engineering, Nanyang Technological University, Singapore 639798, Singapore